Journal of Zhejiang University-SCIENCE A (Applied Physics & Engineering)
ISSN 1673-565X (Print); ISSN 1862-1775 (Online)
www.zju.edu.cn/jzus; www.springerlink.com
E-mail: jzus@zju.edu.cn

Coupled 3D discrete-continuum numerical modeling of pile penetration in sand*

Jian ZHOU[1], Qi-wei JIAN[†‡1], Jiao ZHANG[2], Jian-jun GUO[3]

([1]*Department of Geotechnical Engineering, Tongji University, Shanghai 200092, China*)

([2]*School of Civil Engineering and Transportation, Shanghai Technical College of Urban Management, Shanghai 200432, China*)

([3]*Sichuan Provincial Chuanjian Investigation and Design Institute, Chengdu 610017, China*)

[†]E-mail: jianqiwei1987@gmail.com

Received July 2, 2011; Revision accepted Nov. 2, 2011; Crosschecked Dec. 6, 2011

Abstract: A coupled discrete-continuum simulation incorporating a 3D aspect and non-circular particles was performed to analyze soil-pile interactions during pile penetration in sand. A self-developed non-circular particle numerical simulation program was used which considered sand near the pile as interacted particles using a discrete element method; the sand away from the pile was simulated as a continuous medium exhibiting linear elastic behaviors. The domain analyzed was divided into two zones. Contact forces at the interface between the two zones were obtained from a discrete zone and applied to the continuum boundaries as nodal forces, while the interface velocities were obtained from the continuum zone and applied to the discrete boundaries. We show that the coupled discrete-continuum simulation can give a microscopic description of the pile penetration process without losing the discrete nature of the zone concerned, and may significantly improve computational efficiency.

Key words: Coupled numerical modeling, Discrete-continuum, Micro and macro 3D simulation, Non-circular particles, Pile penetration mechanism

doi:10.1631/jzus.A1100172 **Document code:** A **CLC number:** TU473

1 Introduction

As the foundation design for controlling the settlement of piles is gradually accepted by the academic and engineering fields, it is important to estimate the variation in pile resistance with deformation during pile penetration.

Studies on pile penetration have been conducted using several methods: (1) Theoretical analyzes including the bearing capacity theory (Terzaghi, 1943; Durgunoglu and Mitchell, 1975) and cavity expansion methods (Salgado and Mitchell, 1997; Yu, 2000); (2) Experiments including model tests (Yasufuku and Hyde, 1995; Lehane and Gavin, 2001; Paik and Salgado, 2004) and centrifuge tests (Phillips and Valsangkar, 1987; Bolton and Gui, 1993); (3) Numerical analyses including strain path methods (Baligh, 1985) and finite element methods (Yu *et al*., 2000; Huang *et al*., 2004). However, progress in developing rigorous methods to analyze penetration in sand has been extremely slow due to the dilatant characteristics of sand during shear. Numerical methods may provide a better understanding of the penetration process.

Currently, numerical studies focus mainly on the macroscopic viewpoint of the penetration. Most models of granular materials are based mainly on a continuum assumption, which is used in the small strain theory (De Borst and Vermeer, 1984) or finite deformation theories (Kiousis *et al.*, 1988; Van den Berg *et al.*, 1996). However, the pile penetration

‡ Corresponding author

* Project (No. 90815008) supported by the National Natural Science Foundation of China

mechanism is still not very clear. An alternative tool for studying the penetration mechanism is the discrete element method (DEM) developed by Cundall and Strack (1979), based on discrete mechanics. This numerical analysis technique is very convenient for treating the granular material as a composition of discrete particles and provides a realistic description of granular material on a micro-scale. This has proved to be useful for simulating macroscopic parameters derived from discrete simulation (Masson and Martinez, 2000) and for numerical penetration tests (Tanaka *et al*., 2000; Jiang *et al*., 2006; Lobo-Guerrero and Vallejo, 2007). This discrete approach involving a large number of regular particles is logical and rational but computationally prohibitive and time-consuming. Hence, it is impossible to carry out a discrete simulation containing large numbers of particles.

A coupling method which may address this problem was presented by Felippa and Park (1980) and Park and Felippa (1983), and has been developed rapidly in recent years. Our research group has presented a 2D coupled micro-macro method, which could reduce particle numbers without losing the granular properties of the zone concerned (Jin and Zhou, 2010). Nevertheless, a more realistic modeling is needed which takes account of the properties of real granular materials, i.e., their 3D aspects and the particles' shape. In this paper, a coupled micro-macro 3D simulation of pile penetration in pure sand is carried out to gain new insights into the behavior of the pile penetration process.

2 Preparation for the micro-macro scale coupled simulation

2.1 Discrete and continuum simulation

The discrete simulation based on the DEM can keep track of the motion of individual particles and update any contact with neighboring elements. The code used in this work was PFC3D (Itasca, 2005) which is a recent version of the program BALL developed by Cundall and Strack (1979). In PFC3D, the particles are assumed to be rigid and particle/particle or particle/wall contact involving contact force and relative displacement is taken into account by allowing them to interpenetrate each other. Also, particle motion resulting from any unbalanced force is determined by the application of Newton's second law.

The continuum simulation here is performed by the FLAC3D program (Itasca, 2002). As there are few plastic deformation forces in this zone, and their influences on the DEM domain are insignificant (Guo, 2010), a linear elastic model type was chosen to simulate the behavior of granular material far away from the pile, with two macro mechanical parameters: Young's modulus E, and Poisson's ratio ν. The use of the continuum simulation far away from the impacted area represents a way to minimize the computational constraint since severe degradation phenomena are localized right in the vicinity of the impact.

2.2 Coupling method based on contact between particles and elements

In this study, the DEM is used in the focus domain on a micro-scale, and the finite difference method is used in the surrounding zone on a macro-scale. The contact forces at the boundary follow the principles defined in the DEM. In the continuum elements, the velocities at the contact points are related to the nodal velocities by interpolation, and the contact forces contribute to the nodal forces through weighted values. The coupling is approached using the socket connection of the FLAC and PFC programs.

2.2.1 Contact between the elements and the particles

Coupling is achieved by the exchange of contact forces and velocities between the elements and the particles at the boundary. When individual contact is considered, the contact between the element and the particle can be described by the contact point $x_i^{[C]}$ at the contact surface, which can be defined by the unit normal vector $\boldsymbol{n}_i$. $\boldsymbol{n}_i$ is defined along the straight line which is the shortest distance from the particle's centre to the element at the interface. The contact force can be resolved into two rectangular components: the component of normal vector and the component of tangential vector. The relative displacements of the normal and tangential vectors can be related to the components of contact force by the normal and tangential contact stiffnesses (Fig. 1)

The unit normal vector $\boldsymbol{n}_i$ at the interface is in the direction of the interior normal. The position of the contact point can be obtained from

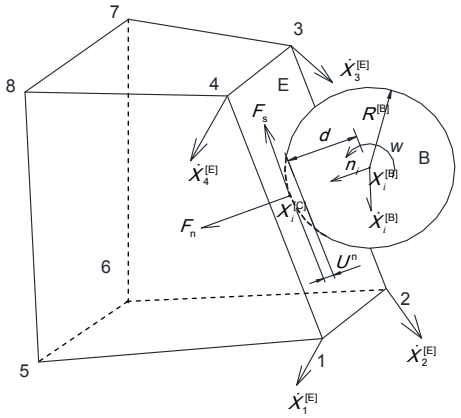

Fig. 1 Contact geometry between a particle and a continuum element

The superscriptions C, B, and E represent contact, ball and element, respectively

$$x_i^{[C]} = x_i^{[B]} + (R_i^{[B]} - (R_i^{[B]} - d)/2)\boldsymbol{n}_i, \tag{1}$$

where d is the distance from the particle's centre $x_i^{[B]}$ to the interface, and $R_i^{[B]}$ is the diameter of the particle.

The contact force at the interface can be resolved into two rectangular components: the component of the normal vector and the component of the tangential vector:

$$\boldsymbol{F}_i^{[C]} = \boldsymbol{F}_{ni}^{[C]} + \boldsymbol{F}_{si}^{[C]}, \tag{2}$$

where $\boldsymbol{F}_{ni}^{[C]}$ is in the normal direction, and $\boldsymbol{F}_{si}^{[C]}$ is in the tangential direction.

The component of normal vector $\boldsymbol{F}_{ni}^{[C]}$ can be calculated by

$$\boldsymbol{F}_{ni}^{[C]} = K^n U^n \boldsymbol{n}_i, \tag{3}$$

where U^n is the contact overlap, $U^n = R_i^{[B]} - d$; and K^n is the normal contact stiffness, which can be evaluated by the contact stiffness model.

The tangential contact forces can be expressed by incrementation. When the contacts come into being, the total tangential contact force is initialized as zero, and then the incrementation of the tangential elastic contact forces can be evaluated by the tangential relative displacement. The motion of the contacts can be considered by monitoring the updating of the normal vector $\boldsymbol{n}_i$ and the position of contacts $x_i^{[C]}$ in each time step. The relative contact velocity at interface V_i is given by

$$V_i = \dot{x}_{i,E}^{[C]} - \dot{x}_{i,B}^{[B]} = \dot{x}_{i,E}^{[C]} - [\dot{x}_i^{[B]} + e_{ijk}\omega_j^{[B]}(x_k^{[C]} - x_k^{[B]})], \tag{4}$$

where $\dot{x}_{i,E}^{[B]}$, $\dot{x}_{i,B}^{[B]}$ are the velocities of element and particle respectively, at the interface, $\dot{x}_i^{[B]}$ is the translational velocity of the particles at contact, $\omega_j^{[B]}$ is the rotational velocity, and e_{ijk} is the permutation symbol, defined as

$$e_{ijk} = \begin{cases} 0, \text{ if 2 indices coincide;} \\ +1, \text{ if } i, j, k \text{ permute like 1, 2, 3;} \\ -1, \text{ otherwise.} \end{cases} \tag{5}$$

Since the overlap between the particles and elements is small, the velocities in continuum elements at the contact points are obtained by interpolating into the neighboring nodal velocities with the type function:

$$\dot{x}_{i,E}^{[C]} = \sum N_j \dot{x}_{i,E}^{j}, \tag{6}$$

$$N_i = (1+\xi_0)(1+\eta_0)/4, \ i = 1,2,3,4, \tag{7}$$

where $\dot{x}_{i,E}^{j}$ is the nodal velocity of element j, N_i is the type function, and $\xi_0 = \xi_i \xi$, $\eta_0 = \eta_i \eta$, ξ_i and η_i are the local coordinates of nodes.

In the 3D model, the interface of the 8-node hexahedral elements is equivalent to a 4-node plane element incorporating three degrees of freedom per node. The velocity of the contact points is obtained by interpolating into the nodal velocity, and the contact forces contribute to the nodal forces through a weight value (Fig. 2).

The contact displacement incrementation per time step is given by

$$\Delta x_{ni}^{[C]} = V_i \Delta t, \tag{8}$$

where Δt is the time step.

The contact displacement incrementation at a contact point can be resolved into two rectangular components: the component of normal vector $\Delta x_{ni}^{[C]}$ and the component of tangential vector $\Delta x_{si}^{[C]}$:

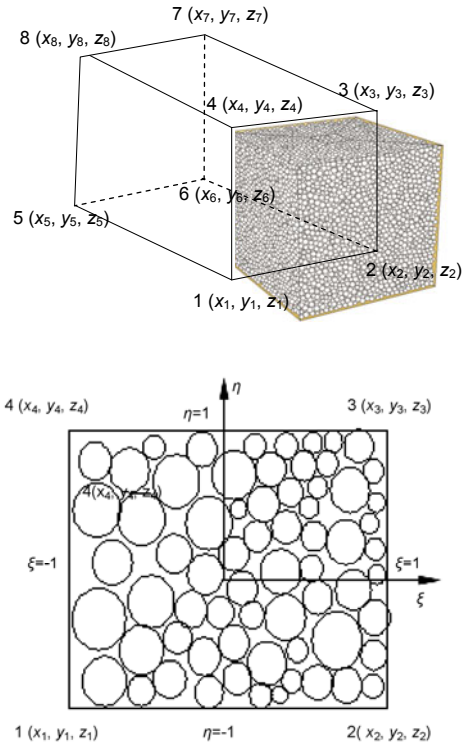

Fig. 2 Particles and elements at the contact interface

$$\begin{aligned}\Delta x_{ni}^{[C]} &= \Delta x_i^{[C]} \boldsymbol{n}_i,\\ \Delta x_{si}^{[C]} &= \Delta x_i^{[C]} - \Delta x_i^{[C]} \boldsymbol{n}_i.\end{aligned} \tag{9}$$

The incrementation of the elastic tangential contact force in each time step Δt is expressed as

$$\Delta F_{si}^{[C]} = -k^s \Delta x_{si}^{[C]}, \tag{10}$$

where k^s is the tangential contact stiffness.

The new tangential contact force component is given by the superposition of the incrementation of the elastic tangential contact force and the tangential contact force component:

$$F_{si}^{[C]} \leftarrow F_{si}^{[C]} + \Delta F_{si}^{[C]} \le \mu F_{ni}^{[C]}, \tag{11}$$

where μ is the friction coefficient.

By Eqs. (3) and (11), the resultant force and resultant moment on contacted particles can be obtained:

$$\begin{aligned}\boldsymbol{F}_i^{[B]} &\leftarrow \boldsymbol{F}_i^{[B]} - \boldsymbol{F}_i^{[C]},\\ \boldsymbol{M}_i^{[B]} &\leftarrow \boldsymbol{M}_i^{[B]} - e_{ijk}\left(x_j^{[C]} - x_j^{[B]}\right)\boldsymbol{F}_k^{[C]},\end{aligned} \tag{12}$$

where $\boldsymbol{F}_i^{[B]}$ and $\boldsymbol{M}_i^{[C]}$ are the superposition of contact forces and the moment of contact forces respectively, on contacted particles; $x_j^{[C]}$ is the coordinates of the contact point, and $x_j^{[B]}$ is the centre of the contacted particle.

In the continuum element at the interface, contact forces contribute to the nodal forces through a weight value, and the total contact force is updated by

$$\boldsymbol{F}_i^{[E,j]} = \boldsymbol{F}_i^{[E,j]} + \boldsymbol{F}_i^{[C]} K_j, \tag{13}$$

where $\boldsymbol{F}_i^{[E,j]}$ is the nodal force of node j in the continuum element at the interface, and K_j, the weight value, is a type function, denoted by N_j.

Due to the small overlap of particles and continuum elements, the influence of the force moment on elements $M = \left|F_{si}^{[C]}\right| U^n / 2$ caused by the tangential contact force is not taken into account.

The contact relationship between the particles and the elements, by which the contact forces and the new positions of particles and nodes can be obtained, is useful for the whole interface of the discrete and continuum domain.

2.2.2 Framework of the coupling simulation

In 3D simulation, 8-noded hexahedral elements are incorporated in continuum simulation and particles are used in discrete simulation. Translation motion in continuum and discrete elements can be expressed as

$$F_i = \sum_C F_C + R^i = m\ddot{x}_i, \tag{14}$$

and the rotational motion in discrete elements is

$$M_3 = \sum_c r_c \times F_c + K^i = I\dot{\omega}_3, \tag{15}$$

where F_i is the total external forces; F_c the contact forces; r_c the direction vector pointing to the particle's centre; m the mass; x_i the displacement; M_3 the total force moment; I the particle's moment of inertia; ω_3 the particle's angular velocity; and R^i and K^i are the external force and the moment of external force, respectively.

The explicit central differencing scheme is used to solve the equations of motion in discrete and continuum elements:

$$\dot{x}_t^{t+\Delta t/2} = \dot{x}_t^{t-\Delta t/2} + \frac{F_i^t}{m}\Delta t,$$
$$\omega_3^{t+\Delta t/2} = \omega_3^{t-\Delta t/2} + \frac{M_3^t}{I}\Delta t. \tag{16}$$

The displacement in the time $t+\Delta t$ is expressed as

$$x_i^{t+\Delta t} = x_i^t + x_i^{t+\Delta t/2}\Delta t. \tag{17}$$

Within each time step, the contact force at the interface between the two domains is updated and then applied back to the two domains. The velocity and relative displacement are evaluated using the motion equation. When the next time step starts, the position of the particles and elements at the interface will firstly be updated through the previous calculation, then the contacts at the interface will be recalculated and distributed back to the two domains before a new round of calculation begins in that time step.

The forces on the particles at the interface contain particle/particle contact forces, external forces, and the particle/interface contact forces. Nodal forces on the elements at the interface contain interior forces caused by the deformation of elements, external forces, and contact forces with particles. The framework of the coupling simulation is illustrated in Fig. 3. The calculation of contacts at the interface will be added to the discrete and continuum coupling simulation.

2.2.3 Achievement of the coupling procedure

The FLAC and PFC programs are explored by Itasca. Both programs have a parallel configuration and socket, which can be further developed. In the coupling simulation, the time steps in FLAC and PFC should keep in step with each other. The use of the socket I/O (input/output) functions may open up the possibility of exchanging data for coupling. At the beginning of each time step, the information on particles and elements at the interface is collected and exchanged using socket functions. The procedures of the coupling simulation are as follows:

(1) Build and initialize the whole model with FLAC code, and then obtain the initial boundary stress in PFC domain;

(2) Generalize the particle flow code model with PFC code, and apply the initial boundary stress obtained in the first step to the boundary of the particle flow code model, then cycle to balance;

(3) Delete the elements of FLAC in PFC domain, open the socket I/O functions as the serve and the client to communicate;

(4) Apply forces to both domains, and cycle to the next time step;

(5) Transport the nodal velocities at the interfaces obtained in FLAC domain to PFC domain with the use of the socket I/O functions;

(6) Obtain the contact forces at interfaces obeying the contact-displacement law, apply contact forces to the particles at interfaces in PFC domain, and convert contact forces to nodal forces which will be applied to elements in FLAC domain;

(7) Cycle the PFC and FLAC model to next time step, back to the fifth step.

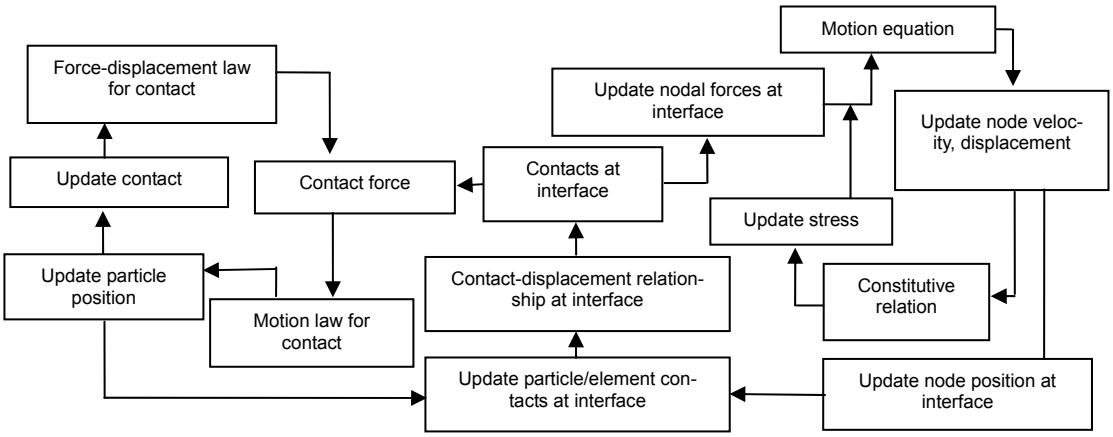

Fig. 3 Flowchart of discrete-continuum coupling calculation

2.3 Self-developed non-circular particle numerical model in discrete simulation

Only circular particles are considered by PFC, but this is not in accordance with the actual shape of sand particles. Considering the limitations of circular particle simulation, our research group has developed an elliptical particle element by using the clump logic in particle flow code (Shi *et al.*, 2008).

In this method, a number of particles can join together as a group of single particles and an arbitrary shape for the group can be constructed by the formation of aggregates (Fig. 4). The particles can either overlaping or not. In the algorithm, we focus on the contacts between groups regardless of the contacts and forces between particles within the groups. As the joint particles group cannot be broken, it is helpful for improving computational efficiency when using the non-circular particle numerical simulation.

To be completely compatible with the porosity of the stress field to the initial state, two basic principles for the conversion from circular to non-circular particles should be obeyed: (1) volume equivalent; (2) mass equivalent.

After several numerical experiments, the results show that two particles could be contacted perfectly provided $1 \le A/B \le 2$, where A and B mean major axis and minor axis of the elliptical clump particle, respectively (Fig. 4). In this study, A/B is taken to be 1.5.

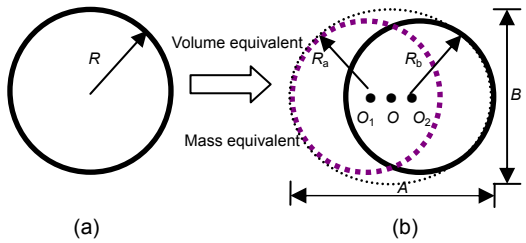

Fig. 4 Circular particle transformed into an elliptical clump particle

(a) Circular particle; (b) Elliptical particle

3 Simulation of pile penetration

3.1 Determination of micro and macro parameters

In our discrete zone, particles are generated as non-circular with uniform distribution while taking account of their shape. The microscopic parameters of particles were obtained from the numerical triaxial compression test. The procedures were as follows:

(1) Adopt a numerical sample as a triaxial test specimen, surrounded by upper and lower flat walls and a cylindrical wall. The non-circlular particles were randomly generated in the cylindrical region (Fig. 5);

(2) Specify the initial porosity by expanding the diameter of the particle;

(3) Set certain microscopic parameters, cycle to initial state of the numerical sample;

(4) Apply triaxial confining pressure using servo-control system;

(5) Apply axial displacement till failure;

(6) Repeat steps (4) and (5) to change the confining pressure.

During the simulation of numerical triaxial test, the microscopic parameters of the test specimen should be adjusted to approach the actual lab test results. After several tests, a more ideal combination of microscopic parameters may be obtained. The radii of the particles ranged from 1.5 to 2.0 mm. The values of the solid density ρ_s, the porosity e, the particle/particle contact stiffness k_n for the normal direction and k_s for the shear direction, the particle/particle friction coefficient f_c, and the particle/element friction coefficient f_b are shown in Table 1.

By using a discrete particle simulation of a triaxial compression test, the macro-parameters of the granular material adopted in the continuum model can be obtained from knowledge of the particle properties and the microscopic distribution of particles (Table 2).

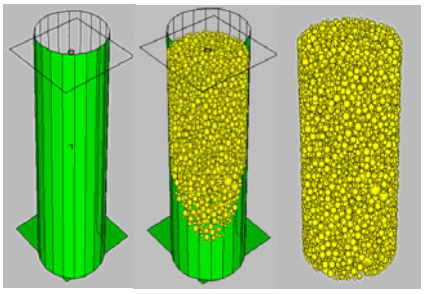

Fig. 5 Triaxial test specimen

Table 1 Values of microscopic parameters of numerical samples

Parameter	Value	Parameter	Value
ρ_s (kg/m^3)	2650	k_n/k_s	8
e	0.36	f_c	0.7
k_n (N/m)	1×10^7	f_b	1.0

Table 2 Values of macroscopic parameters of numerical samples

Parameter	Value	Parameter	Value
ρ_d (kg/m^3)	1630	G (MPa)	36.92
E (MPa)	44.3	K (MPa)	17.04
ν	0.3		

Fig. 6 compares the results from numerical and lab tests. The macroscopic parameters of the sample obtained from the numerical triaxial compression test are close to the lab test results and the set of microscopic parameters is suitable.

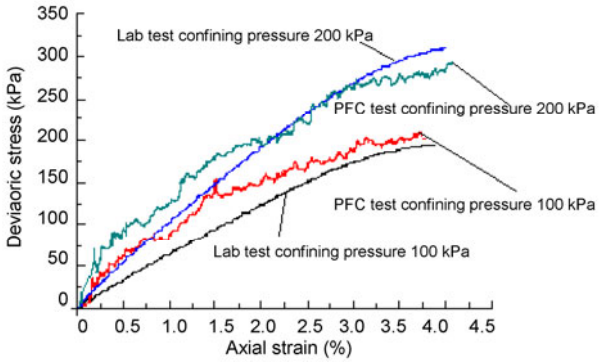

Fig. 6 Comparison between the PFC and lab tests

3.2 Numerical procedure

Due to the 10*g*-level employed in the centrifuge test (Guo, 2010), the numerical model is 10 times larger than the centrifuge model. The coupling model has dimensions of 625 cm×625 cm×900 cm, and is filled with 26700 non-circular particles and 21280 eight-node hexahedral elements (Fig. 7). The pile is simulated as stiff walls with a constant velocity in PFC3D domain, and the length and diameter of the pile are 400 and 25 cm, respectively. The geometry of the discrete model is cylindrical with 3.5 times the diameter and 1.8 times the length of the pile. The pile penetration depth (S/D) increment is normalized as 10% of the pile diameter for each penetration step, with a constant penetration velocity, i.e., ΔS/D=0.1.

The numerical pile penetration procedure consists of pushing a pile into the discrete zone with a constant penetration velocity, and calculating the linear elastic zone away from the pile, while interchanging unbalanced wall forces in PFC3D and grid node velocities in FLAC3D using the socket I/O functions. The interface between the discrete and continuous zones is divided into segments. These segments are treated as velocity boundaries in PFC3D, while in FLAC3D mean stresses are applied to such segments corresponding to FLAC's grid sides. Zero velocity boundaries during penetration are applied to the surrounding and bottom sides of the continuous brick.

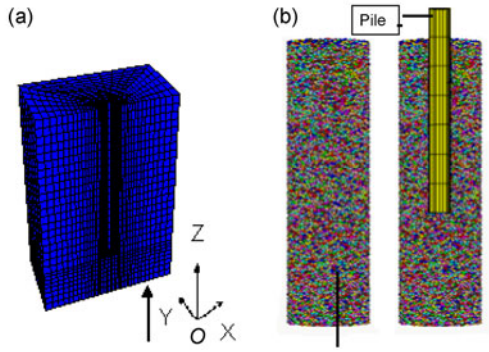

Fig. 7 Continuum and discrete models
(a) One-half continuous zone depicted by FLAC3D; (b) Discontinuous zone simulated as a set of particles

4 Numerical validation and results analysis

4.1 Numerical simulations validation

Compared with the simulation using particle flow code, the coupled simulation reduced the particle numbers and significantly improved computational efficiency. Table 3 shows a comparison of computational efficiency between the coupled simulation and the particle flow code simulation.

Table 3 Comparison of computational efficiency

Parameter	Coupled simulation	Particle flow code simulation
Particle number	26700	61000
Grid	21280	–
Time step (s)	5×10^{-7}	5×10^{-7}
Time (d)	22	55

Pile tip resistance obtained by the coupled simulation tends to reach a limit as the normalized S/D approaches 0.7, and then increases slightly with S/D (Fig. 8), corresponding better to the previous results from centrifuge tests (Guo, 2010).

This consistency verifies the correctness of the coupled numerical simulation of pile penetration from

a macroscopic view, and proves that the coupled simulation may explain the macro-micro mechanism of soil variation around the pile tip during penetration in qualitative analysis.

4.2 Vertical stresses in the zone governed by the continuum model

In the coupled simulation, the vertical stress fields in the continuous zone show variation with different penetration depths (Fig. 9). Corresponding to the increase in penetration depth, the vertical stress field zone develops gradually, and tends to reach a steady state as the pile tip resistance reaches a limit when the penetration depth is approximately 0.7 times the diameter of pile.

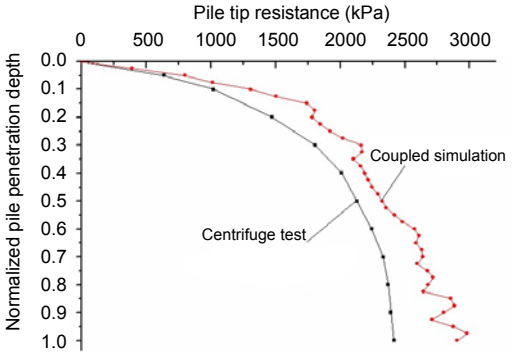

Fig. 8 Pile tip resistance along with pile penetration depth

4.3 Numerical analysis on micro-scale

4.3.1 Particle/particle and particle/pile contact forces at the pile tip

Pure sand close to the pile tip exhibits nonlinear properties. It is convenient to simulate penetration in this zone by using the DEM which provides a microscopic perspective of the mechanism of sand variation with pile penetration.

To show if the coupled method and the particle flow code method can produce very similar results, the particle/particle and particle/pile contact forces at the pile tip were analyzed and compared. The trends shown by the variation in the particle contact forces obtained by the coupled method agree with those shown by the particle flow code simulation (Fig. 10). The maximum contact forces exist in close proximity to the pile tip and then decrease quickly away from the tip. It is obvious that the particle/particle and particle/pile contact forces develop with increasing penetration depth and slow down when the pile tip resistance reaches a limit.

4.3.2 Distribution of sand porosity around the pile

As discussed above, the pile tip resistance reaches a limit when the normalized penetration depth equals 0.7 times the pile diameter. The porosity of sand near the pile was analyzed as S/D=0.3 and 0.7, then compared with the results in particle flow code simulation.

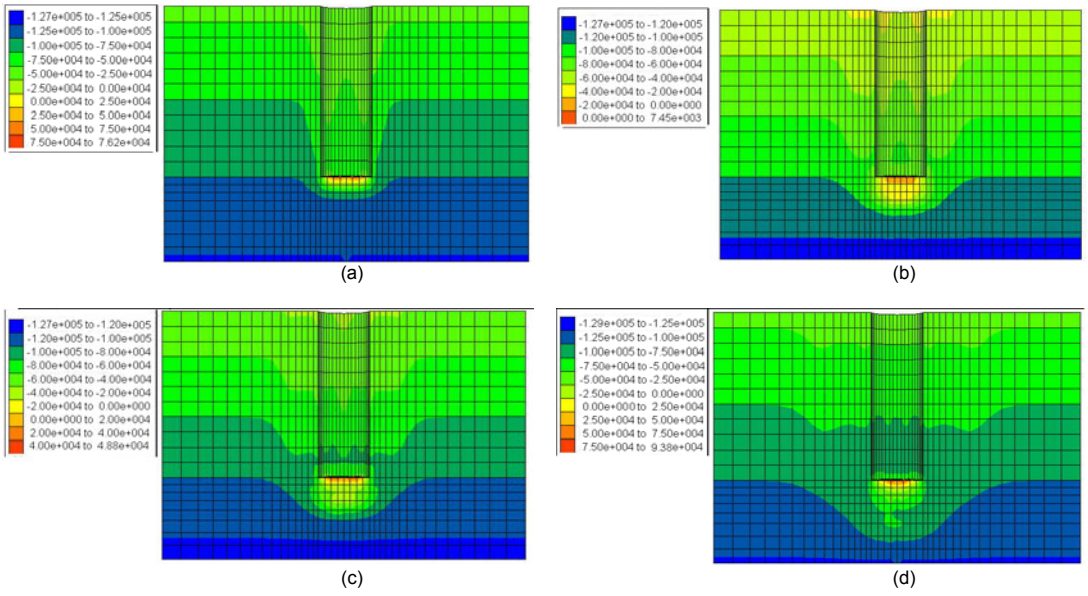

Fig. 9 Vertical stress fields in the continuous zone during penetration (unit: Pa)
(a) S/D=0.1; (b) S/D=0.5; (c) S/D=0.7; (d) S/D=1.0

Fig. 11 presents the distributions of sand porosities obtained by the coupled method and particle flow code method at different penetration depths. Note that the distributions of sand porosities are similar in both methods at the same normalized penetration depth. During the penetration process, a high density core forms beneath the pile footing. Degradation phenomena are localized where the sand exerts an impact on the pile, sand porosity decreases and the sand becomes compacted from a microscopic viewpoint. Above the pile tip, a shear zone can be found because of the slide between the pile and the sand caused by frictional resistance, sand porosity increases and then dilatancy occurs. The main features of the sand porosity are consistent with those observed in particle flow code simulation.

4.3.3 Traced representative particles

A coupled simulation has proved to be feasible, from which the results obtained on a micro-scale are in agreement with those from particle flow code simulation. For further analysis of the mechanism of pile penetration, the displacements of four representative particles in coupled simulation were traced (Fig. 12).

Particles 1 and 2 are located in the pile's vertical central axis, and the vertical distance between the two is equal to the diameter of the pile. Particles 1, 3 and 4 are chosen at the same horizontal level, from which the vertical distance to the bottom of the pile is one-half the diameter of the pile, the same as the horizontal distance between the neighboring particles. Fig. 12 shows the variations in the displacement of

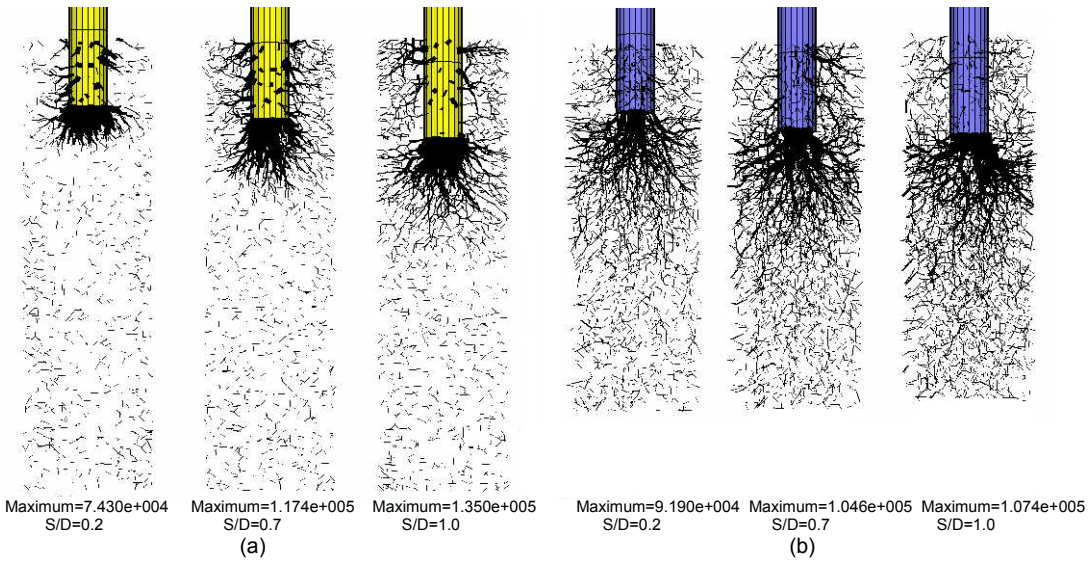

Fig. 10 Comparison of variations in contact forces with S/D between the coupled simulation (a) and particle flow code simulation (b) (unit: N)

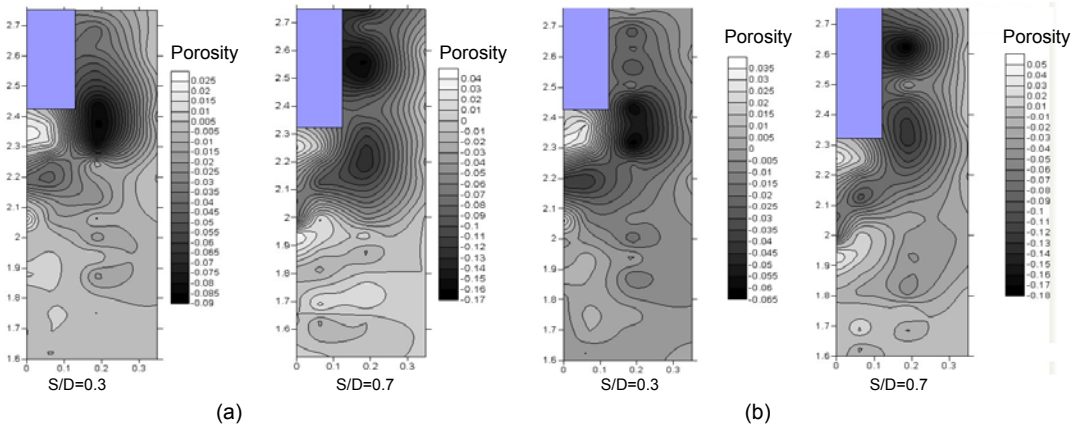

Fig. 11 Comparison of the porosity of sand between the coupled simulation (a) and particle flow code simulation (b)

the four traced particles in the *X*-direction and the *Z*-direction.

In Figs. 13a and 13b, Particles 1, 3 and 4 are chosen at the same horizontal level. In the horizontal direction, Particles 3 and 4 move sidewards, and the displacement of Particle 3 is much larger than that of Particle 4. Particle 1 remains nearly unmoved. In the vertical direction, Particles 1 and 3 move downwards, and the displacement of Particle 1 is much larger than that of Particle 3. Particle 4 remains unmoved.

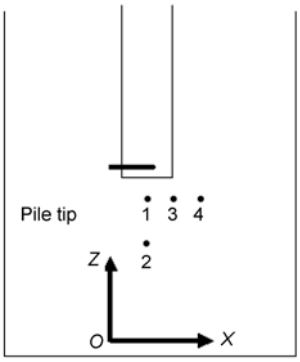

Fig. 12 Locations of traced particles below the pile

Comparing Figs. 13c and 13d, where Particles 1 and 2 are located at the same vertical plane, both remain nearly unmoved in the horizontal direction, but move downward in the vertical direction, and the vertical displacement of Particles 1 is much larger than that of Particles 2. This can be explained by the distance from the pile.

Tracing representative particle displacements demonstrates well that pile penetration is a dynamic process and shows how the sand has been influenced during pile penetration.

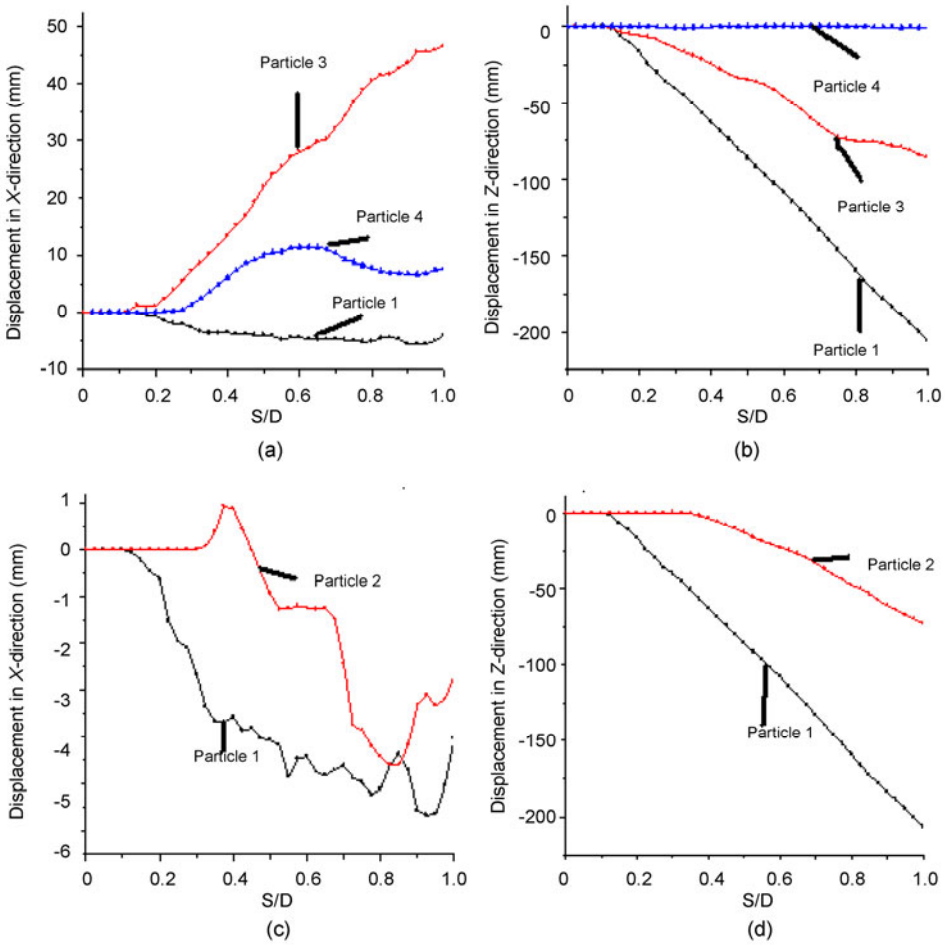

Fig. 13 Displacements of traced particle

Particles 1, 3 and 4 in (a) *X*-direction and (b) *Z*-direction; Particles 1 and 2 in (c) *X*-direction and (d) *Z*-direction

5 Conclusions

In this research, a coupled simulation incorporating the 3D aspect and non-circular particle shapes has been applied in analyzing the process of pile penetration from microscopic and macroscopic points of view, which combines the advantages of both the discrete and continuum methods and explores the exchange model of interface velocities and contact forces between the discrete and continuum boundaries.

The main conclusions can be drawn as follows:

1. The coupled simulation can significantly improve computational efficiency. The use of the discrete simulation, from which the macro-scale parameters of granular materials can be derived, can incorporate the discrete nature and particle shapes of sand, and thus provides a perspective on discerning the microscopic mechanism of penetration into sands. The continuum simulation governing the domain away from the pile efficiently reduces particle numbers.

2. The coupling of the procedure is achieved by the exchange of vectors at the boundary. The coupling model may dynamically reveal the pile penetration process on a micro-scale providing new insights into sand behavior. Contact forces at the interface were obtained from the discrete zone and applied to the continuum boundaries as nodal forces, while the interface velocities were obtained from the continuum zone and applied to the discrete boundaries.

3. During pile penetration in sand, particle/particle and particle/pile contact forces develop with increasing penetration depth and remain when the pile tip resistance reaches a limit when S/D equals 0.7; a high density core exists beneath pile tip point, and degradation phenomena are localized where the sand exerts an impact on the pile; at the pile footing point, the sand becomes loose and dilatancy may occur. This is in good agreement with results from particle flow code simulation on a micro-scale.

4. The coupled method may provide a foundation for the further study of the macro-micro mechanisms of soil variation around a pile tip in the course of penetration.

References

Baligh, M.M., 1985. Strain path method. *Journal of Geotechnical Engineering*, **111**(9):1108-1136. [doi:10.1061/(ASCE)0733-9410(1985)111:9(1108)]

Bolton, M.D., Gui, M.W., 1993. The study of relative density and boundary effects for cone penetration tests in centrifuge. Research Report CUED/D-SOILS/TR256, Department of Engineering, Cambridge University, UK.

Cundall, P.A., Strack, O.D.L., 1979. A discrete numerical model for granular assemblies. *Geotechnique*, **29**(1):47-65. [doi:10.1680/geot.1979.29.1.47]

De Borst, C., Vermeer, P.A., 1984. Finite element analysis of static penetration tests. *Geotechnique*, **34**(2):199-210. [doi:10.1680/geot.1984.34.2.199]

Durgunoglu, H.T., Mitchell, J.K., 1975. Static Penetration Resistance of Soils. Proceedings of the ASCE Specialty Conference on In-Situ Measurements of Soil Properties, Raleigh, **1**:151-189.

Felippa, C.A., Park, K.C., 1980. Staggered transient analysis procedures for coupled-field mechanical systems: formulation. *Computer Methods in Applied Mechanics and Engineering*, **24**(1):61-111. [doi:10.1016/0045-7825(80)90040-7]

Guo, J.J., 2010. Study on Macro-scale and Meso-scale Mechanism of Penetration Deformation of Pile in Layered Soil. PhD Thesis, Department of Geotechnical Engineering, Tongji University, China (in Chinese).

Huang, W., Sheng, D., Sloan, S.W., Yu, H.S., 2004. Finite element analysis of cone penetration in cohesionless soil. *Computers and Geotechnics*, **31**(7):517-528. [doi:10.1016/j.compgeo.2004.09.001]

Jiang, M.J., Yu, H.S., Harris, D., 2006. Discrete element modelling of deep penetration in granular soils. *International Journal for Numerical and Analytical Methods in Geomechanics*, **30**(4):335-361. [doi:10.1002/nag.473]

Itasca, 2002. FLAC User Manual, Version 5.0. Itasca Consulting Group Inc., USA.

Itasca, 2005. PFC User Manual, Version 3.0. Itasca Consulting Group Inc., USA.

Jin, W., Zhou, J., 2010. A Coupled Micro-Macro Method for Pile Penetration Analysis. GeoShanghai International Conference, Shanghai, China, p.234-239.

Kiousis, P.D., Voyiadjis, G.Z., Tumay, M.T., 1988. A large strain theory and its application in the analysis of the cone penetration mechanism. *International Journal for Numerical and Analytical Methods in Geomechanics*, **12**(1):45-60. [doi:10.1002/nag.1610120104]

Lehane, B.M., Gavin, K.G., 2001. Base resistance of jacked pipe piles in sand. *Journal of Geotechnical and Geoenvironmental Engineering*, **127**(6):473-480. [doi:10.1061/(ASCE)1090-0241(2001)127:6(473)]

Lobo-Guerrero, S., Vallejo, L.E., 2007. Influence of pile shape and pile interaction on the crushable behavior of granular materials around driven piles: DEM analyses. *Granular Matter*, **9**(3-4):241-250. [doi:10.1007/s10035-007-0037-3]

Masson, S., Martinez, J., 2000. Multiscale simulations of the mechanical behaviour of an ensiled granular material. *Mechanics of Cohesive-Frictional Materials*, **5**(6):425-442. [doi:10.1002/1099-1484(200008)5:6<425::AID-CFM103>3.0.CO;2-V]

Paik, K., Salgado, R., 2004. Effect of pile installation method on pipe pile behavior in sands. *Geotechnical Testing Journal*, **27**(1):78-88. [doi:10.1520/GTJ11391]

Park, K.C., Felippa, C.A., 1983. Partitioned Analysis of Coupled Systems. Computational Methods for Transient Analysis, North-Holland, p.157-219.

Phillips, R., Valsangkar, A.J., 1987. An Experimental Investigation of Factors Affecting Penetration Resistance in Granular Soils in Centrifuge Modelling. Research Report CUED/D-SOILS/TR210, Department of Engineering, Cambridge University, UK.

Salgado, R., Mitchell, J.K., Jamiolkowski, M., 1997. Cavity expansion and penetration resistance in sand. *Journal of Geotechnical and Geoenvironmental Engineering, ASCE*, **123**(4):344-354. [doi:10.1061/(ASCE)1090-0241(1997)123:4(344)]

Shi, D.D., Zhou, J., Liu, W., Jia, M., 2008. Numerical simulation for behaviors of sand with non-circular particles under monotonic shear loading. *Chinese Journal of Geotechnical Engineering*, **30**:1361-1362.

Tanaka, H., Momozu, M., Oida, A., Yamazaki, M., 2000. Simulation of soil deformation and resistance at bar penetration by the distinct element method. *Journal of Terramechanics*, **37**(1):41-56. [doi:10.1016/S0022-4898(99)00013-0]

Terzaghi, K., 1943. Theoretical Soil Mechanics. Wiley, New York.

Van den Berg, P., De Borst, R., Huetink, H., 1996. An Eulerean finite element model for penetration in layered soil. *International Journal for Numerical and Analytical Methods in Geomechanics*, **20**(12):865-886. [doi:10.1002/(SICI)1096-9853(199612)20:12<865::AID-NAG854>3.0.CO;2-A]

Yasufuku, N., Hyde, A.F.L., 1995. Pile end-bearing capacity in crushable sands. *Geotechnique*, **45**(4):663-676. [doi:10.1680/geot.1995.45.4.663]

Yu, H.S., 2000. Cavity Expansion Methods in Geomechanics. Kluwer Academic Publishers, the Netherlands.

Yu, H.S., Herrmann, L.R., Boulanger, R.W., 2000. Analysis of steady cone penetration in clay. *Journal of Geotechnical and Geoenvironmental Engineering, ASCE*, **126**(7):594-605. [doi:10.1061/(ASCE)1090-0241(2000)126:7(594)]